Local Field Enhancement of Mid-Infrared Light in an Integrated Photonic-Plasmonic Structure

Andrea Blanco-Redondo, Paulo Sarriugarte, Angel Garcia-Adeva, Joseba Zubia, and Rainer Hillenbrand

***Abstract*—We numerically study the local field enhancement of mid-infrared light beating the diffraction limit in an integrated photonic-plasmonic structure. The light is locally transferred from a photonic crystal waveguide to a metallic transmission line on top of it. The transmission line connects the two sections of the photonic crystal waveguide in a passage configuration. The field intensity is locally enhanced in the transmission line passage by a factor larger than 50, with a power transfer efficiency of 33%. This passage structure holds the promise of enabling highly sensitive miniaturized sensing schemes and mid-infrared spectroscopy equipment.**

***Index Terms*—Local field enhancement, metallic transmission lines, mid-infrared photonics, photonic crystal waveguides, photonic-plasmonic coupling.**

I. Introduction

THE recent progress in photonic-plasmonic integration [1]–[9] has paved the way towards the hybrid photonic chip. A new level of functionality may be achieved by combining the outstanding control capabilities over light signals of photonic crystal waveguides (PhC-wgs) [10]–[13] with the capacity of plasmonic waveguides to confine light in a volume much smaller than its wavelength [14]–[19]. Whereas PhC-wgs suffer from higher propagation losses than conventional dielectric waveguides (∼5dB/cm for PhC-wgs [20], [21] and up to ∼1 dB/cm for silicon wires [22], [23]), the design flexibility of PhC-wgs provides us with more degrees of freedom to achieve effective coupling to plasmonic waveguides. The field of plasmonics in the mid-infrared (mid-IR) part of the spectrum [24]–[27] could particularly benefit from integration with PhC-wgs because new functionalities for hybrid waveguide-plasmon infrared sensor might be achieved. PhC-wgs provide further control on the spatial, temporal, and spectral course of photons, increasing the available on-chip functionality.

Manuscript received June 27, 2014; revised October 24, 2014; accepted December 7, 2014. Date of publication December 17, 2014; date of current version January 23, 2015. This work was supported in part by Euskampus and the Basque Government under Projects ETORTEK "nanoiker" (IE11-304), SAIOTEK (S-PE12UNO43), GIC07/156-IT-343-07, and AIRHEM III, the Spanish Ministerio de Ciencia e Innovación under Projects MAT2012-36580 and TEC2012-37983-C03-01, and the University of the Basque Country under Project UFI11/16. The work of P. Sarriugarte was supported by the "Ikertzaileen Prestakuntza eta Hobekuntzarako Programa" promoted by the Department of Education, Universities and Research of the Basque Government.

A. Blanco-Redondo is with the Aerospace Unit of the Industry and Transport Division of Tecnalia, Parque Tecnológico de Bizkaia, E-48170 Zamudio, Spain (e-mail: andrea.blanco@tecnalia.com).

P. Sarriugarte is with the Nanooptics Group, CIC nanoGUNE, 20018 Donostia, Spain (e-mail: p.sarriugarte@nanogune.eu).

A. Garcia-Adeva and J. Zubia are with the Departmento de Fisica Aplicada I, E.T.S. Ingeniería de Bilbao, 48103 Bilbao, Spain (e-mail: angel.garcia-adeva@ehu.es; joseba.zubia@ehu.es).

R. Hillenbrand is with the Nanooptics Group, CIC nanoGUNE, 20018 Donostia, Spain, and also with the IKERBASQUE, Basque Foundation for Science, 48011 Bilbao, Spain (e-mail: r.hillenbrand@nanogune.eu).

Color versions of one or more of the figures in this paper are available online at http://ieeexplore.ieee.org

Digital Object Identifier 10.1109/JLT.2014.2382560

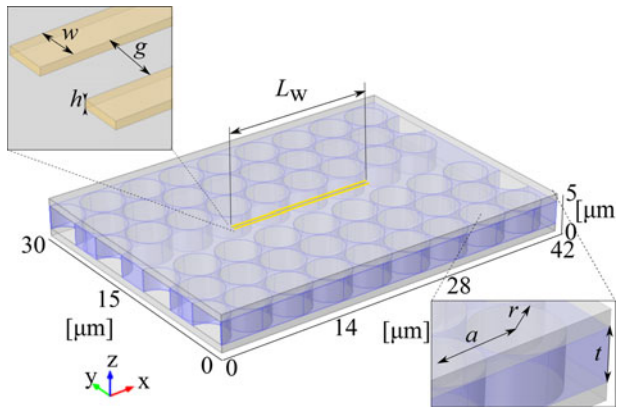

Fig. 1. Schematic of the hybrid structure with the TL passage: the TL, situated at the center of the surface of the silicon PhC-wg ($a = 4.9$ μm; $r = 0.48 \cdot a$; $t = 0.6 \cdot a$; $n_{\mathrm{Si}} = 3.46$ and $n_{\mathrm{air}} = 1$ at $\lambda_0 = 10$ μm), consists of two parallel gold wires ($w = 200$ nm, $h = 40$ nm, $L_w = 17$ μm, $g = 300$ nm; $n_{\mathrm{Au}} = 12.59 + i59$ at 10 μm).

We recently demonstrated the efficient coupling of mid-IR light from a silicon PhC-wg to a metallic transmission line (TL) formed by two parallel gold nanowires [8]. In [8] an input plane wave with a wavelength of $\lambda_0 = 10$ μm was initially coupled to the transverse magnetic (TM)-like mode of the PhC-wg and then gradually transferred to the symmetric mode of the TL, along a coupling length of $L_c \approx 8$ μm. Subsequently it showed a periodic energy transfer between the symmetric mode of the TL and TM-like PhC-wg mode, with a computed oscillation period of $L_0 \approx 18$ μm. Here, building on the basis of our previous results, we numerically demonstrate that mid-IR light within the PhC-wg can be locally transformed into a surface wave on the TL and back to the PhC-wg. To enable this demonstration we propose a TL passage connecting two sections of a PhC-wg. Furthermore, we study the optimization of the structure in terms of power transfer efficiency, providing physical explanations on the coupling process and the loss mechanisms.

II. A TL Passage

The proposed hybrid structure is depicted in Fig. 1. The PhC-wg relies on a silicon air-suspended photonic crystal with a hexagonal lattice constant of $a = 4.9$ μm, air hole radii of $r = 0.48 \cdot a$, and silicon slab thickness of $t = 0.6 \cdot a$. The waveguide is created by removing a row of holes (W1 type).The TL passage consists of two parallel gold nanowires of width $w = 200$ nm,

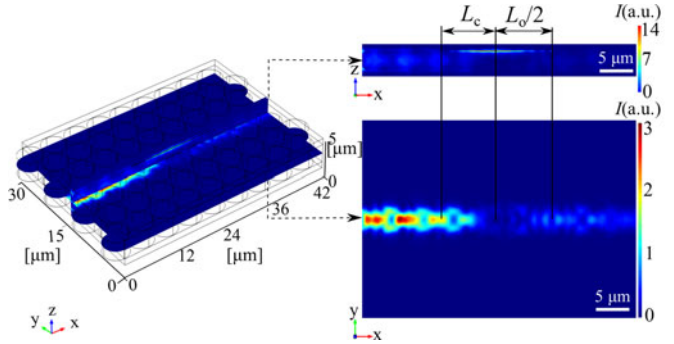

Fig. 2. Normalized electric field intensity obtained by exciting the hybrid structure with a wave polarized in *z*: on the left, a view of the hybrid structure with *I* at two parallel *x*-*z* planes at the center of each wire and a *x*-*y* plane at the center of the silicon slab; on the right, individual views of one of the *x*-*z* planes at the center of a wire and a subsection of the *x*-*y* plane at the center of the silicon centered in the PhC-wg ($Lc \approx 8$ μm and $Lo \approx 18$ μm).

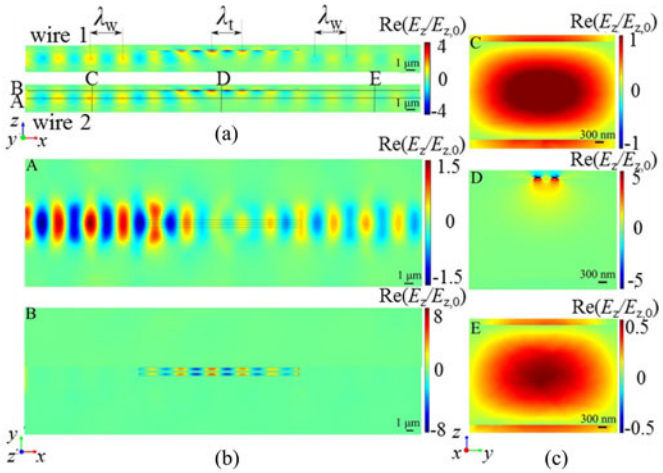

Fig. 3. Normalized real part of the electric field *z*-component ($\mathrm{Re}(E_z/E_{z,0})$) in: (a) two *x*-*z* slices at the center of each gold wire, (b) *x*-*y* slices at the center of the PhC-wg (A) and below the surface of the wires (B); (c) *y*-*z* slices before (C), in the middle (D), and after (E) the TL.

and thickness $h = 40$ nm, which are separated by an air gap $g = 300$ nm.

The length of the TL passage is initially fixed to $L_w = L_c + L_o/2 = 17$ μm, since the periodic energy transfer observed in [8] suggests that this length could maximize the energy transfer from the TL back to the PhC-wg. At a distance L_w from the beginning of the TL, the field energy is mostly within the PhC-wg and thereby it is foreseeable that this scheme minimizes the amount of loss at the TL termination.

The propagation of mid-IR light along the proposed structure is investigated using the COMSOL Multiphysics implementation of the finite element method (FEM) [28] and complemented by the Opti finite differences in time domain (FDTD) implementation of the FDTD method. In Fig. 2 the electric field intensity in the structure is shown at several spatial planes. As expected from the results in [8], the maximum energy transfer to the TL occurs at a distance of $L_c = 8$ μm from the beginning of the TL. At the end of the TL, the energy is efficiently coupled back to the PhC-wg and continues its propagation towards the end of the hybrid structure. Specifically, 33% of the power present in the PhC-wg before the TL passage is confined in a cross section of area 1400 nm $\times$ 500 nm centered in the TL, demonstrating a clear beating of the diffraction limit.

By evaluating the distribution of the electric field *z*-component $(\mathrm{Re}(E_z/E_{z,0}))$ in Fig. 3(a) and (b), we verified that the effective wavelength in the PhC-wg is the same before and after the TL, $\lambda_w \approx 3.46$ μm, whereas the effective wavelength in the TL is $\lambda_t \approx 3.32$ μm. Fig. 3(c) shows three cross sections of the field distribution $\mathrm{Re}(E_z/E_{z,0})$ along the propagation direction, before the TL (cross section C), at the position of maximum energy transfer to the TL (cross section D) and after the TL (cross section E). At cross section D, the field nearly vanishes inside the PhC-wg, indicating that most of the energy is converted to the TL mode. After back-coupling to the PhC-wg, the field distribution reveals the typical TM-like mode of the PhC-wg (cross section E). The field magnitude, however, is reduced from (C) to (E) due to radiation loss along the PhC-wg and energy dissipation in the metal wires of the TL. The portion of the electric field that is radiated to the substrate and cladding in the PhC-wg is observed in (C) and (E) by the red stripes at the silicon-air interfaces.

The local intensity enhancement factor (LIEF) is computed as the maximum value of the electric field intensity on the surface of the TL in contact with air at the point of maximum energy transfer, normalized to the maximum value of the field intensity at the surface of the PhC-wg just before the TL passage. Large local field enhancements have demonstrated huge potential to provide strong light-matter interaction for enhanced optical nonlinearities [29] or surface-enhanced molecular spectroscopy [30] amongst others. For our TL passage we calculate an LIEF ≈ 53, indicating potential to become an efficient mid-IR sensing device and to contribute to the miniaturization of mid-IR spectroscopy equipment.

III. The Optimization of the Structure

We next study the *x*-component of the normalized Poynting vector $S_x(x)$ in the 17 μm-long TL passage for a better understanding of the power loss mechanisms and for optimization of the TL length in terms of power transference. Fig. 4(a) shows S_x at several cross sections x_i along the propagation direction. Before and after the TL (x_1, x_2, x_5, x_6), the energy flows within the PhC-wg. Along the TL passage (x_3, x_4), the energy propagates as a surface mode and is strongly concentrated around the TL. The energy transfer to the TL reaches its maximum at a distance of L_c from the beginning of the TL (point x_3 in Fig. 4(b)) before the energy couples gradually back into the PhC-wg.

In order to optimize the length of the TL passage we have to consider two competing aspects: maximum field enhancement requires maximum power transfer to the TL, which occurs at L_c; on the other hand, as energy propagating along metallic TLs suffers from dissipation, we should minimize the length of the TL. Bearing this compromise in mind, we calculated the power as a function of the propagation distance *P*(*x*) for several TL lengths, L_w, between $L_c = 8$ μm and the end of

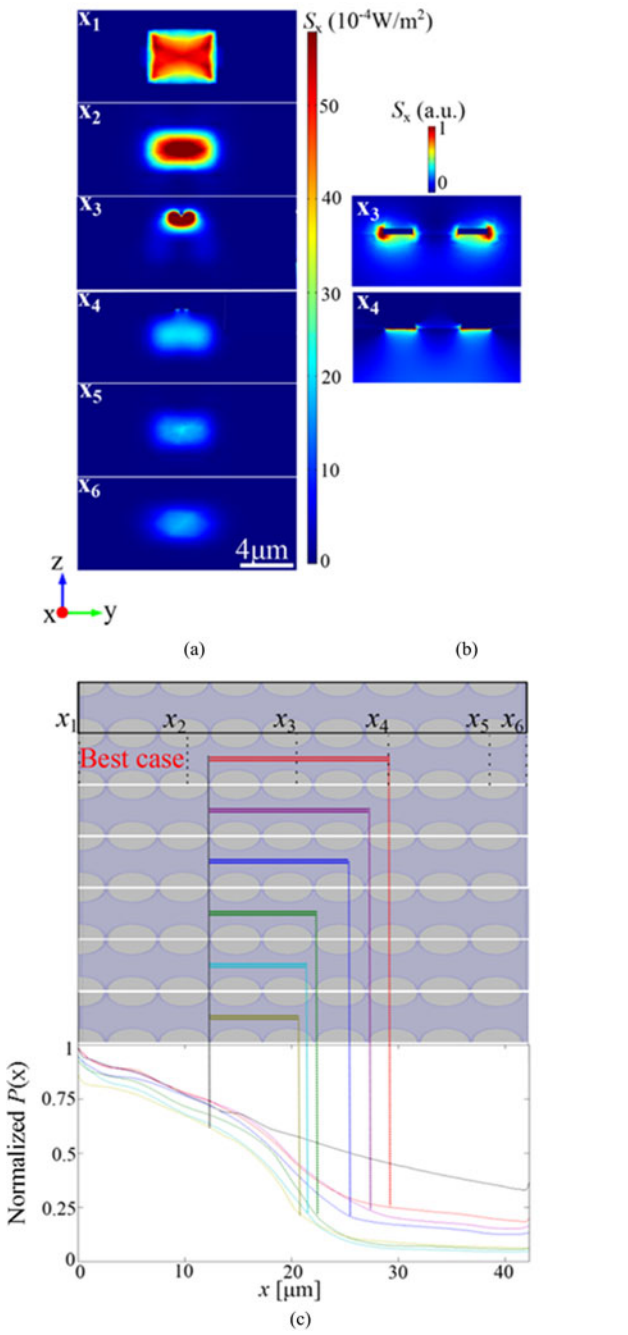

Fig. 4. Optimization of the transmission line length. (a) X-component of the normalized Poynting vector $S_x(x)$ at several cross sections along the propagation x-direction (x_1-x_6) for the 17 μm-long TL passage; (b) Detail of the $S_x(x)$ around the TL (for x_3 and x_4); (c) Power $P(x)$ passing through the cross section in x-direction as a function of the position x for TL lengths of: 8 μm (olive green), 9 μm (cyan), 10 μm (dark green), 13 μm (blue), 15 μm (purple), 17 μm (red), and 0 μm (black).

the first power transference period $L_c + L_o/2 = 17$ μm (curves in color in Fig. 4(c)). $P(x)$ is computed by integrating $S_x(x)$ at every step of the propagation distance. For comparison, the black curve in Fig. 4(c) shows the power $P(x)$ in the PhC-wg without a metallic TL on its surface. When the energy is being transferred from the PhC-wg to the TL, the slope of $P(x)$ significantly increases due to dissipation of energy in the metal wires. Conversely, the slope of $P(x)$ decreases when the light is coupling back to the PhC-wg, since in absence of the metal wires only radiation losses occur. This general trend of $P(x)$ is similar for all TL lengths. Nevertheless the quantitative behavior of $P(x)$ differs significantly depending on the TL length. When L_w decreases, the $P(x)$ curves shift to smaller values and the total loss $\Delta P = P(x_1) - P(x_6)$ increases. This fact may seem counterintuitive since the dissipation is expected to decrease for shorter propagation distances along the metallic TL. This observation can be explained by back-reflection at the open-end termination of the TL, which becomes more significant as the amount of power concentrated around the TL at its termination increases. The back-reflection has two noticeable effects. First, it shifts the $P(x)$ curves to lower values, as now back-reflected energy is transferred in the backward propagating direction and therefore contributes negatively to the power flow. Second, the slope of $P(x)$ along the TL becomes steeper. The explanation for this is that the energy back-reflected at the open-end termination eventually reaches the other open-end TL termination where, in turn, part of the energy will be back-reflected. This results in energy passing several times through the TL, where dissipation in the metal wires occurs, thus increasing the total loss per length unit, i.e. the slope of $P(x)$, along the TL. Indeed, we find that ΔP is minimized for the 17 μm-long TL, confirming that $L_w = L_c + L_o/2$ is the optimum TL length. The efficient coupling from the PhC-wg to the TL and vice versa can be explained by making use of the directional coupling principle. A detailed application of such principle to the coupling between these two particular structures was presented in [8].

We define the power transfer efficiency (PTE) of the hybrid structure as the ratio between the output and input power: $\mathrm{PTE} = P(x_6)/P(x_1)$. The PTE allow us to compare the performance of the TL passage for the different TL lengths: in the best case we obtain $\mathrm{PTE} = 0.2$ but this figure gradually decreases towards the worst case ($L_w = L_c = 8$ μm) where $\mathrm{PTE} = 0.05$. Note that the PTE not only depends on the coupling efficiency from the PhC-wg to the TL and vice versa, but also from the overall power loss, including radiation loss and dissipation along the metal length. In the best case we obtain 20% of end-to-end energy transfer, even after the wave has undergone strong local field enhancement in the TL. This finding holds great promise for the development of infrared waveguides with enhanced sensitivity to their immediate environment (e.g. low-concentration analytes), since this level of output power is readily measurable with optical detection schemes.

IV. Conclusion

We proposed and theoretically studied an integrated photonic-plasmonic structure that allows for local field enhancement of mid-IR light on a metallic TL passage on a PhC-wg. The interest in this hybrid structure lies in the fact that light can travel a long distance along the relatively low-loss PhC-wg, be locally confined in the TL, to finally couple back to the PhC-wg and continue its low-loss propagation. The intensity of the field is enhanced by a factor of 53 on the TL passage, facilitating strong interaction of the mid-IR light with matter. With a coupling

efficiency of 33%, this scheme presents an exciting potential for practical applications in biosensing [31], [32], optical interconnects [33], and IR spectroscopy [34] among others.

We have considered the PhC-wg TM-mode coupling to the symmetric mode of the TL, for different TL lengths. The best performance, in terms of the energy transferred to end of the hybrid structure, occurs when the TL is terminated at the point where most energy is transferred back into the PhC-wg, even if this is the longest TL considered. This configuration minimizes back-reflection and radiation at the TL termination.

This type of hybrid structure comprising PhC-wgs and metallic TL passages could become a basic building block for waveguide sensors in the mid-IR and contribute to the miniaturization of mid-IR spectroscopy equipment.

REFERENCES

[1] J. T. Kim, Y.-J. Yu, H. Choi, and C.-G. Choi, "Graphene-based plasmonic photodetector for photonic integrated circuits," *Opt. Exp.*, vol. 22, no. 1, pp. 803–809, 2014.

[2] D. Mao, M. Li, W. Y. Leung, K.-M. Ho, and L. Donga, "Photonic-plasmonic integration through the fusion of photonic crystal cavity and metallic structure," *J. Nanophoton.*, vol. 5, no. 1, pp. 059501-1–059501-6, 2011.

[3] C. Delacour, S. Blaize, P. Grosse, J. M. Fedeli, A. Bruyant, R. Salas-Montiel, G. Lerondel, and A. Chelnokov, "Efficient directional coupling between silicon and copper plasmonic nanoslot waveguides: Toward metal-oxide-silicon nanophotonics," *Nano Lett.*, vol. 10, no. 8, pp. 2922–2926, 2010.

[4] Y. Song, J. Wang, Q. Li, M. Yan, and M. Qiu, "Broadband coupler between silicon waveguide and hybrid plasmonic waveguide," *Opt. Exp.*, vol. 18, no. 12, pp. 13173–13179, 2010.

[5] B. Fan, F. Liu, X. Wang, Y. Li, K. Cui, X. Feng, and Y. Huang, "Integrated sensor for ultra-thin layer sensing based on hybrid coupler with short-range surface plasmon polariton and dielectric waveguide," *Appl. Phys. Lett.*, vol. 102, no. 6, pp. 061109-1–061109-4, 2013.

[6] R. M. Briggs, J. Grandidier, S. P. Burgos, E. Feigenbaum, and H. A. Atwater, "Efficient coupling between dielectric-leaded plasmonic and silicon photonic waveguides," *Nano Lett.*, vol. 10, pp. 4851–4857, 2010.

[7] R. F. Oulton, V. J. Sorger, D. A. Genov, D. F. Pile, and X. Zhang, "A hybrid plasmonic waveguide for subwavelength confinement and long-range propagation," *Nature Photon.*, vol. 2, pp. 496–500, 2008.

[8] A. Blanco-Redondo, P. Sarriugarte, A. Garcia-Adeva, J. Zubia, and R. Hillenbrand, "Coupling mid-infrared light from a photonic crystal waveguide to metallic transmission lines," *Appl. Phys. Lett.*, vol. 104, pp. 011105-1–011105-5, 2014.

[9] F. Liu, Y. Li, R. Wan, Y. Huang, X. Feng, and W. Zhang, "Hybrid coupling between long-range surface plasmon polariton mode and dielectric waveguide mode," *J. Lightw. Technol.*, vol. 29, no. 9, pp. 1265–1273, May 2011.

[10] A. Blanco-Redondo, C. Husko, D. Eades, Y. Zhang, J. Li, T. F. Krauss, and B. J. Eggleton, "Observation of soliton compression in silicon photonic crystals," *Nature Commun.*, vol. 5, no. 3160, pp. 1–8, 2014.

[11] A. Mekis, J. Chen, I. Kurland, S. Fan, P. Villeneuve, and J. Joannopoulos, "High transmission through sharp bends in photonic crystal waveguides," *Phys. Rev. Lett.*, vol. 77, no. 18, pp. 3787–3790, 1996.

[12] Y. Vlasov, M. O'Boyle, H. Hamann, and S. McNab, "Active control of slow light on a chip with photonic crystal waveguides," *Nature*, vol. 438, no. 7064, pp. 65–69, 2005.

[13] A. Blanco-Redondo, D. Eades, J. Li, S. Lefrancois, T. F. Krauss, B. J. Eggleton, and C. Husko, "Controlling free-carrier temporal effects in silicon by dispersion engineering," *Optica*, vol. 1, no. 5, pp. 299–306, 2014.

[14] S. Maier, *Plasmonics: Fundamentals and Applications*. New York, NY, USA: Springer, 2007.

[15] D. Gramotnev and S. Bozhevolnyi, "Plasmonics beyond the diffraction limit," *Nature Photon.*, vol. 4, no. 2, pp. 83–91, 2010.

[16] V. Brar, M. Jang, M. Sherrott, J. Lopez, and H. Atwater, "Highly confined tunable mid-infrared plasmonics in graphene nanoresonators," *Nano Lett.*, vol. 13, no. 6, pp. 2541–2547, 2013.

[17] E. Ozbay, "Plasmonics: Merging photonics and electronics at nanoscale dimensions," *Science*, vol. 311, no. 5758, pp. 189–193, 2006.

[18] A. Rusina, M. Durach, K. Nelson, and M. Stockman, "Nanoconcentration of terahertz radiation in plasmonic waveguides," *Opt. Exp.*, vol. 16, no. 23, pp. 18576–18589, 2008.

[19] J. Schuller, E. Barnard, W. Cai, Y. Jun, J. White, and M. Brongersma, "Plasmonics for extreme light concentration and manipulation," *Nature Mater.*, vol. 9, no. 3, pp. 193–204, 2010.

[20] E. Kuramochi, M. Notomi, S. Hughes, A. Shinya, T. Watanabe, and L. Ramunno, "Disorder-induced scattering loss of line-defect waveguides in photonic crystal slabs," *Phys. Rev. B*, vol. 72, pp. 161 318–161 321, 2005.

[21] L. O'Faolain, X. Yuan, D. McIntyre, S. Thoms, H. Chong, R. M. De La Rue, and T. F. Krauss, "Low-loss propagation in photonic crystal waveguides," *Electron. Lett.*, vol. 42, no. 25, pp. 1454–1455, 2006.

[22] M. Gnan, S. Thoms, D. S. Macintyre, R. M. De La Rue, and M. Sorel, "Fabrication of low-loss photonic wires in silicon-on-insulator using hydrogen silsesquioxane electron-beam resist," *Electron. Lett.*, vol. 44, pp. 115–116, 2008.

[23] J. Cardenas, C. B. Poitras, J. T. Robinson, K. Preston, L. Chen, and M. Lipson, "Low loss etchless silicon photonic waveguides," *Opt. Exp.*, vol. 17, pp. 4752–4757, 2009.

[24] M. Schnell, P. Alonso-González, L. Arzubiaga, F. Casanova, L. E. Hueso, A. Chuvilin, and R. Hillenbrand, "Nanofocusing of mid-infrared energy with tapered transmission lines," *Nature Photon.*, vol. 5, pp. 283–287, 2011.

[25] P. Krenz, R. Olmon, B. Lail, M. Raschke, and G. Boreman, "Near-field measurement of infrared coplanar strip transmission line attenuation and propagation constants," *Opt. Exp.*, vol. 18, no. 21, pp. 21678–21686, 2010.

[26] S. Law, D. Adams, A. Taylor, and D. Wassermann, "Mid-infrared designer metals," *Opt. Exp.*, vol. 20, no. 11, pp. 12155–12165, 2012.

[27] R. Stanley, "Plasmonics in the mid-infrared," *Nature Photon.*, vol. 6, pp. 409–411, 2012.

[28] I. Andonegui and A. J. Garcia-Adeva, "The finite element method applied to the study of two-dimensional photonic crystals and resonant cavities," *Opt. Exp.*, vol. 21, pp. 4072–4092, 2013.

[29] P.-Y. Chen, C. Argyropoulos, and A. Alu, "Enhanced nonlinearities using plasmonic nanoantennas," *Nanophotonics*, vol. 1, pp. 221–233, 2012.

[30] Y. Li, L. Su, C. Shou, C. Yu, J. Deng, and Y. Fang, "Surface-enhanced molecular spectroscopy (SEMS) based on perfect-absorber metamaterials in the mid-infrared," *Sci. Rep.*, vol. 3, pp. 1–8, 2013.

[31] P. Debackere, S. Scheerlinck, P. Bienstman, and R. Baets, "Surface plasmon interferometer in silicon-on-insulator: Novel concept for an integrated biosensor," *Opt. Exp.*, vol. 14, no. 16, pp. 7063–7072, 2006.

[32] R. Adato, A. Yanik, J. Amsden, D. Kaplan, F. Omenetto, M. Hong, S. Erramilli, and H. Altug, "Ultra-sensitive vibrational spectroscopy of protein monolayers with plasmonic nanoantenna arrays," *Proc. Nat. Academy Sci. United States Amer.*, vol. 106, no. 46, pp. 19 227–19 232, 2009.

[33] D. Miller, "Device requirements for optical interconnects to silicon chips," *Proc. IEEE*, vol. 97, no. 7, pp. 1166–1185, Jul. 2009.

[34] F. Huth, A. Chuvilin, M. Schnell, I. Amenabar, R. Krutokhvostov, S. Lopatin, and R. Hillenbrand, "Resonant antenna probes for tip-enhanced infrared near-field microscopy," *Nano Lett.*, vol. 13, no. 3, pp. 1065–1072, 2013.

Authors' biographies not available at the time of publication.